J. Fluid Mech. (2024), *vol*. 994, A4, doi:10.1017/jfm.2024.629

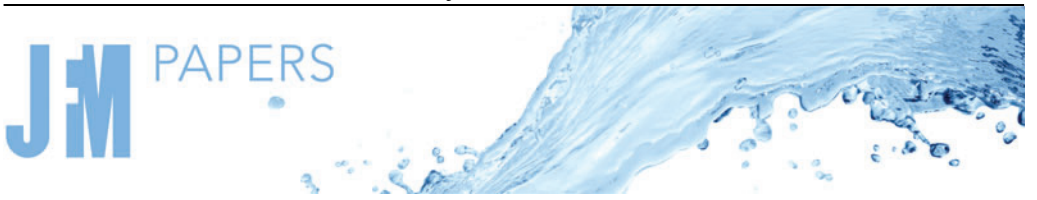

Thermal boundary layer dynamics in low-Prandtl-number Rayleigh–Bénard convection

Nayoung Kim[1],†, **Felix Schindler**[1], **Tobias Vogt**[1] **and Sven Eckert**[1],†

[1]Institute of Fluid Dynamics, Helmholtz-Zentrum Dresden-Rossendorf, 01328 Dresden, Germany

(Received 6 May 2024; revised 13 June 2024; accepted 15 July 2024)

In this experimental study, we explore the dynamics of the thermal boundary layer in liquid metal Rayleigh–Bénard convection, covering the parameter ranges of $0.026 \leq$ Prandtl numbers (Pr) ≤ 0.033 and Rayleigh numbers (Ra) up to 2.9×10^9. Our research focuses on characterising the thermal boundary layer near the top plate of a cylindrical convection cell with an aspect ratio of 0.5, distinguishing between two distinct regions: the shear-dominated region around the centre of the top plate and a location near the side wall where the boundary layer is expected to be affected by the impact or ejection of thermal plumes. The dependencies of the boundary layer thickness on Ra at these positions reveal deviating scaling exponents with the difference diminishing as Ra increases. We find stronger fluctuations in the boundary layer and increasing deviation from the Prandtl–Blasius–Pohlhausen profile with increasing Ra, as well as in the measurements outside the centre region. Our data illustrate the complex interplay between flow dynamics and thermal transport in low-Pr convection.

Key words: Bénard convection, plumes/thermals, boundary layer structure

1. Introduction

Rayleigh–Bénard (RB) convection, characterised by the natural circulation of a fluid between two horizontal plates subjected to a temperature difference, is a fundamental phenomenon in fluid dynamics with significant implications for various industrial and geophysical processes (Rayleigh 1916; Siggia 1994; Bodenschatz, Pesch & Ahlers 2000; Ahlers, Grossmann & Lohse 2009; Chillà & Schumacher 2012). A fundamental parameter in characterising RB convection (RBC) is the Rayleigh number ($Ra = g\beta\Delta TH^3/(\nu\kappa)$), representing the ratio of the buoyancy and viscous forces in the fluid. Here, g is the acceleration due to gravity, β is the coefficient of thermal expansion, ΔT is the temperature

† Email addresses for correspondence: n.kim@hzdr.de, s.eckert@hzdr.de

difference between the plates, H is the distance between the plates, ν is the kinematic viscosity and κ is the thermal diffusivity.

The dynamics of the thermal boundary layer (BL) in RBC plays a crucial role in understanding heat transfer mechanisms because the main temperature drop occurs across the BLs which therefore constitute the main resistance for global heat transport (Shraiman & Siggia 1990; Grossmann & Lohse 2000; Sun, Cheung & Xia 2008). In recent years, significant attention has been paid to investigations of the BL dynamics (Wagner, Shishkina & Wagner 2012; Zhou & Xia 2013; Scheel & Schumacher 2014). A special feature of the RBC is that, unlike channel flow, the fluid does not flow continuously along the wall. Three different regions result from the fact that thermal plumes coming from the bulk impinge at the plate (plume impact), and detach at a certain distance from the impact zone (plume ejection), whereas in geometries of laterally confined RBC, the detachment area usually occurs at the opposite end of the plate. Impact and ejection zones are connected by a shear flow across the central area (shear-dominated) (van der Poel *et al.* 2015; Schumacher *et al.* 2016; Scheel & Schumacher 2017; Pandey 2021). The local thickness of the thermal BL is the smallest just after the impact zone and grows in the large-scale circulation (LSC) plane towards the opposite sidewall (Wagner *et al.* 2012; Pandey 2021). Furthermore, the mean temperature profile near the wall displays deviations from the Prandtl–Blasius–Pohlhausen (PBP) profile, a phenomenon particularly pronounced with smaller Prandtl numbers ($Pr = \nu/\kappa$) and larger Ra (van Reeuwijk, Jonker & Hanjalić 2008; Shishkina *et al.* 2015; Ching *et al.* 2019; Tai *et al.* 2021). At higher Ra, these deviations are evident across all three regions (Zhou *et al.* 2010, 2011; Scheel, Kim & White 2012; Shi, Emran & Schumacher 2012; Stevens *et al.* 2012; Wang, He & Tong 2016; Wang *et al.* 2018). Although dynamic rescaling (Zhou & Xia 2010) improves the agreement in the shear and impact region, significant deviations persist, especially in the ejection region (Pandey 2021).

At low Prandtl numbers, thermal diffusion dominates over viscous effects, leading to different BL dynamics compared with higher-Pr fluids. The thermal BL thickness in low-Pr fluids exceeds that of the viscous BL, exposing it to direct interaction with the turbulent flow. Previous studies, including those by Scheel & Schumacher (2016), Schumacher *et al.* (2016), Scheel & Schumacher (2017) and Pandey (2021), extensively explored these dynamics through numerical investigations. Scheel & Schumacher (2017) conducted high-resolution direct numerical simulations at Pr values of 0.005 and 0.021, focusing on statistical quantities such as energy dissipation rates and BL thickness scales. They found that the critical Ra for transitioning to fully turbulent BLs decreases as Pr decreases. The numerical results by Scheel & Schumacher (2017) and Pandey (2021) suggest that BLs in low-Pr convection remain transitional rather than fully turbulent within a Rayleigh number range $Ra \leq 10^{10}$, although increasing fluctuations are observed with increasing Ra.

While numerical simulations enable valuable insights, experimental investigations provide empirical evidence and are crucial for validating computational models. So far, the study by Naert, Segawa & Sano (1997) is the only one we are aware of that experimentally measures the BL thickness in liquid metal convection. The authors used a movable thermocouple to determine the temperature profile in mercury at the centre of the top plate and examined different approaches for determining the BL thickness. Here, our study aims to experimentally investigate thermal BL dynamics in turbulent liquid metal RBC and provides the first experimental data comparing the thermal BL characteristics both inside and outside the shear-dominated region. We analyse temperature profiles,

fluctuation statistics and scaling behaviour, and compare our experimental findings with existing numerical studies.

2. Thermal BL dynamics in liquid metal convection

2.1. *Local vertical temperature gradient in two distinct regions*

The experimental set-up has been thoroughly described in our previous work (Schindler *et al.* 2022). The cylindrical cell has an aspect ratio Γ of 0.5, with dimensions $D =$ 320 mm and $H = 640$ mm. Two copper plates on the upper and lower sides are in contact with the eutectic alloy GaInSn, enabling the investigation of very low Pr values ranging from 0.026 to 0.033. The variation in Pr arises from the temperature sensitivity of both ν and κ, which comes into play as the mean bulk temperature in the convection cell changes with Ra. Our specific focus here lies in analysing the thermal BL structure near the top cold plate. Figure 1(*a*) shows the sensor arrangement configured for that purpose. Two ultrasonic Doppler velocimetry (UDV) sensors are positioned at a distance of $0.016H$ from the top plate to measure the horizontal velocity of the LSC, u_{lsc}, at their cross-section. For measurements of the thermal gradient in the fluid near the top plate, two thermocouple arrays are embedded in the top plate at distances of $0.02D$ and $0.33D$ away from the centre. Each of these arrays contains 10 individual thermocouples, their exact vertical positions are shown in figures 1(*c*) and 1(*d*).

Examples of the temperature data obtained from these two arrays at $Ra = 3.7 \times 10^8$ are depicted as probability density functions (PDFs) in figures 1(*c*) and 1(*d*), respectively. Here, we use the normalised temperature defined as $\Theta = (T - T_{cold})/(T_{bulk} - T_{cold})$, where T_{cold} denotes the top plate temperature, and T_{bulk} is the mean bulk temperature obtained by averaging the temperatures of the top and bottom plates, $T_{bulk} = (T_{cold} + T_{hot})/2$. Three distinct zones can be identified in the temperature profiles measured at the centre (figure 1*c*): within the thermal BL, at the edge of the thermal BL and outside of the BL. The PDFs near the plate are narrow and feature temperatures lower than those of the ambient fluid, confirming their location within the thermal BL. The temperature distributions exhibit an almost Gaussian shape in this area, which means there is only a minimal influence from the bulk flow. It is interesting to note the presence of negative values of Θ in this zone, indicating that the values measured by the thermocouple arrays are sometimes lower than T_{cold}. This occurs because the thermal boundary conditions are generally not ideal in liquid metal convection experiments, even when using copper heat exchanger plates. At some point, the heat conduction in the copper plates can no longer compensate for the temperature fluctuations in the fluid quickly enough. For example, Horanyi, Krebs & Müller (1999) observed large-scale temperature fluctuations in liquid sodium, which they attributed to an interplay between convective heat transport in the sodium and the conductive equalisation of temperature fluctuations in the adjacent copper plates. Moving to the next zone above this area, the PDFs appear significantly wider and thus suggest an area at the edge of the thermal BL in which the shear flow along the plate is already gaining influence. Finally, we identify a mixing zone, where the measured temperature data are distributed around a constant background temperature at $\Theta = 1$. The skewness in the PDFs observed in this zone is likely attributed to the presence of large-scale thermal plumes and associated turbulent mixing, which cause significant temperature fluctuations and lead to asymmetry in the temperature distributions.

Figure 1(*d*) illustrates that the temperature PDFs recorded by the second thermocouple array near the side wall show only minor variations with respect to their maximal values and appear flatter and broader compared with the centre region. This can be interpreted

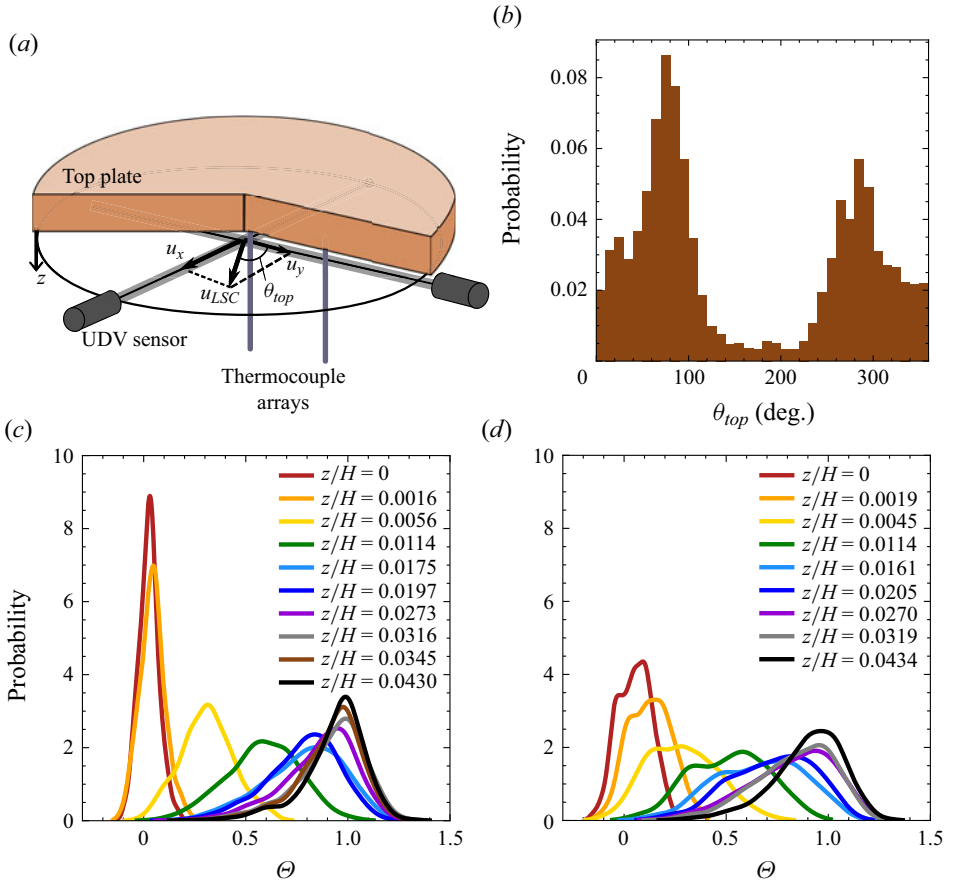

Figure 1. (*a*) Schematic of the experimental set-up with thermocouple arrays and UDV sensors. (*b*) Probability distribution of the LSC direction along the top plate for $Ra = 3.7 \times 10^8$, and probability distribution of temperature data from thermocouple arrays for the same Ra, at the centre of the plate (*c*) and near the side wall (*d*).

as an initial indication that the flow influence and related fluctuations in the thermal BL are becoming stronger when the measuring position changes from the centre towards the side wall. While it is evident that the centre of the plate corresponds to the shear-dominated region, the dominance of the LSC-induced shear flow parallel to the copper plate decreases towards the periphery where effects due to plume impact and ejection at the top plate also come into play.

The UDV sensors are used to determine the LSC direction along the top plate according to the procedure suggested by Zürner *et al.* (2019). Figure 1(*b*) presents an exemplary PDF for $Ra = 3.7 \times 10^8$. Here, the location of the thermocouple array near the side wall is aligned with 0°. Highly turbulent and transient LSC structures with constant changes in flow direction along the plates were observed by flow measurements in the same set-up (Wondrak *et al.* 2023). Nevertheless, one or two preferred directions often emerge (for example, here at 75° and 285°), but these vary from experiment to experiment and are therefore difficult to predict. This means that, at different times, our off-centre thermocouple array can be located either upstream (in the impact region) or downstream (in the ejection region) of the LSC, or even to the side of the LSC plane.

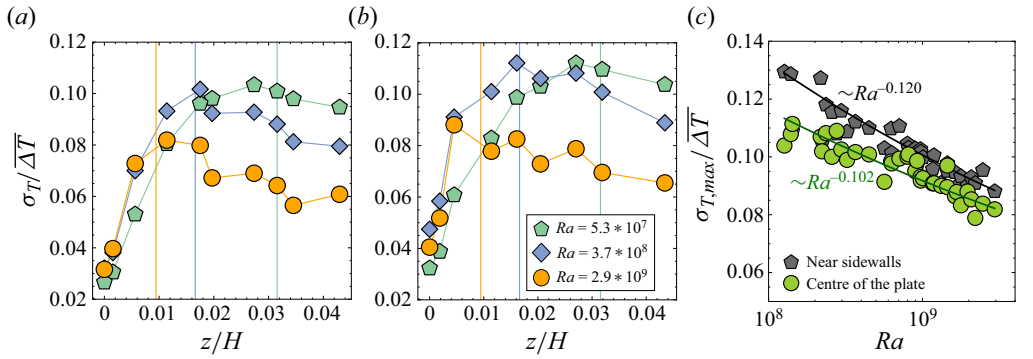

Figure 2. Temperature fluctuation profile in the centre (*a*) and near-wall (*b*) regions. Vertical lines with corresponding colours represent the mean thermal BL thicknesses, $H/(2Nu)$. (*c*) Maximum value of temperature fluctuations normalised by ΔT as a function of Ra.

2.2. *Statistics of the temperature profiles*

For both thermocouple arrays, we compute the root mean square value of the temperature fluctuations which is defined as $\sigma_T(z) = \langle (T - \langle T \rangle)^2 \rangle^{1/2}$, where $\langle\rangle$ indicates time-averaging, and normalise it by the temperature difference between the lower and upper plates $\langle \Delta T \rangle$. These root-mean-square values would be negligible in a laminar BL (Wang *et al.* 2018), but our data in figure 2 suggest that the BL is not entirely laminar. According to previous studies (Zhou & Xia 2013; Scheel & Schumacher 2016; Pandey 2021) temperature fluctuations are smallest within the thermal BL, reach their maximum at the edge of the BL, and decline in the bulk region. The location of $\sigma_{T,max}$ can be considered as the position at the edge of the thermal BL where the characteristic temperature profile meets the ambient fluid. For both measuring positions at the centre and the near-wall region, figures 2(*a*) and 2(*b*) show $\sigma_{T,max}$ occurring close to the mean thermal BL thickness, defined as $H/(2Nu)$ (Ahlers *et al.* 2009; Shishkina & Thess 2009; Chillà & Schumacher 2012). A reduction in the BL thickness with increasing Ra is reflected by the reduction in the distance between $\sigma_{T,max}$ and the top plate at $z = 0$. At the highest Ra considered here, $\sigma_{T,max}$ appears to be closer to the plate in the near-wall region than in the centre, whereas the locations of the $\sigma_{T,max}$ are similar in both regions for lower Ra. This rough observation does not seem to be consistent with the results of Pandey (2021), who found a significant thickening of the BL thickness in the ejection zone. However, Pandey (2021) was able to focus his evaluation on the ejection area by moving the measurement points along with the changing LSC plane. We do not have this possibility in the experiment, so we detect a temporal mixture of plume ejection, plume impact and situations in which we measure outside the LSC plane. Pandey (2021) also observed a clear decreasing trend of the BL thickness in the ejection region for increasing Ra.

In figure 2(*c*), we plot the normalised values $\sigma_{T,max}$ as a function of Ra. The exponent of the slope is $Ra^{-0.102}$ for the centre region and $Ra^{-0.120}$ for the side wall region. Especially in the side wall region, this scaling is similar to the recently reported value of -0.118 (Samuel *et al.* 2024), even though their value derives from spatial averaging and their configuration (Cartesian domain with $\Gamma = 4$) differs from that considered in this study. However, previous experimental studies with $\Gamma = 0.5$ (Castaing *et al.* 1989; Wu & Libchaber 1992; Niemela *et al.* 2000) have reported steeper exponents for the central region, approximately -0.144 to -0.147, indicating a stronger dependence on Ra. Additionally, Samuel *et al.* (2024) found that the exponent can vary depending on the

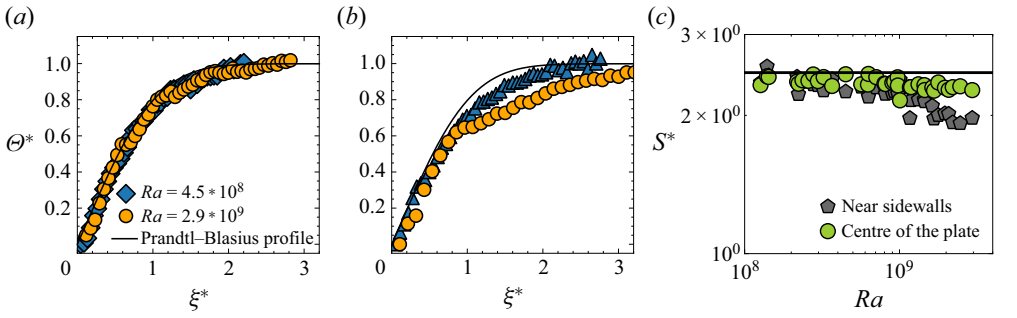

Figure 3. Dimensionless mean temperature profiles as functions of $z/\delta_T(x,t)$ in the centre (a) and near-wall (b) regions. (c) Shape factor S as a function of Ra. The horizontal line denotes the shape factors for the Prandtl–Blasius case ($S \sim 2.47$ for $0.026 \leq Pr \leq 0.033$).

spatial range considered, with their values changing to -0.140 in the bulk region. Here, we focus solely on the maximum temperature fluctuation values near the plate.

The decline in $\sigma_{T,max}/\Delta T$ is explained by Pandey (2021) with the argument that, with increasing Ra, the temperature difference between the plate and the ambient fluid at the edge of the BL decreases which is confirmed by our temperature profiles presented in figure 3(b). This should also reduce the temperature difference between the bulk fluid and the plumes that are formed. Correspondingly, the decrease of $\sigma_{T,max}$ is particularly pronounced at the off-centre position, as plume ejection events are expected to occur only near the side wall, not at the centre. Moreover, figure 2(c) shows that $\sigma_{T,max}$ is larger in the near-wall region compared with the centre region across the entire range of Ra examined here. This is to be expected, as the influence of the shear flow decreases the further away the observation point is from the centre of the plate. Large-scale velocity fluctuations associated with plume impact or ejection are becoming more relevant near the side wall. Due to the small Pr, this is directly reflected in the behaviour of the thermal BL, indicating a starting mixing between the BL and the turbulent bulk flow. In contrast, in the shear-dominated region, where no significant velocity components normal to the plate surface occur, there is less exchange between thermal BL and bulk flow.

The averaged temperature profiles beneath the top plate are plotted in figures 3(a) and 3(b). Many previous studies have shown that dynamically rescaled profiles can provide an intuitive comparison with the PBP profile (Zhou *et al.* 2011; Scheel *et al.* 2012; Shi *et al.* 2012; Stevens *et al.* 2012; Wang *et al.* 2016, 2018). A time-averaged temperature profile in a fixed reference frame as a function of the height z contains mixed dynamics with contributions from inside and outside the BL range, as the BL thickness is constantly changing during the measurement. To achieve a clear separation of those dynamics, Zhou & Xia (2010) studied BL quantities within a time-dependent frame that varied with the instantaneous BL thickness. The rescaled vertical distances and the averaged temperature profiles in the dynamic frame are defined as

$$\xi^*(t) = z/\delta_T(x,t), \tag{2.1}$$

$$\Theta^*(\xi^*) = \langle \Theta(z,t)|_{z=\xi^*(t)\delta_T(x,t)} \rangle. \tag{2.2}$$

Here, the instantaneous local thermal BL $\delta_T(x,t)$ is obtained using the slope method (Zhou *et al.* 2011; Scheel *et al.* 2012; Wagner *et al.* 2012), where $\delta_T(x,t)$ is the distance from the plate to an intersection point where the line with the slope of the temperature profile directly at the plate meets the bulk temperature. Here, $\sigma_{T,max}$ is used to specify the number of data points used for calculating the temperature slope within the BL

($0 \leq z \leq z(\sigma_{T,max})$). The number of selected sensors depends on Ra since the position of $\sigma_{T,max}$ varies with Ra, but this number for a given Ra remains fixed over time.

Previous studies show that the dynamically rescaled temperature profile agrees well with the PBP profile in the impact and shear-dominated regions, indicating a laminar behaviour of the BL in these regions (Zhou & Xia 2010; van der Poel *et al.* 2015; Pandey 2021). In contrast, the profile deviates significantly from the PBP profile in the ejection region due to stronger turbulent fluctuations. Consistent with these previous studies, our measurements in the shear-dominated region demonstrate a very good agreement with the PBP profile for all Ra (see figure 3*a*), whereas significant deviations from the PBP profile are observed for the off-centre position (see figure 3*b*). Here, the difference to the PBP profile increases with growing Ra, indicating an increase in disturbances impairing the laminar character of the BL.

To quantitatively investigate the deviation of the temperature profile from the PBP profile, we calculate the shape factor S^* from the temperature profile in the dynamic frame, which is defined as (Scheel *et al.* 2012; Scheel & Schumacher 2017; Pandey 2021)

$$\delta_d^* = \int_0^\infty \left(1 - \frac{\Theta^*}{\Theta^*_{max}}\right) \mathrm{d}\xi^*, \tag{2.3}$$

$$\delta_m^* = \int_0^\infty \left(1 - \frac{\Theta^*}{\Theta^*_{max}}\right) \frac{\Theta^*}{\Theta^*_{max}} \mathrm{d}\xi^*, \tag{2.4}$$

$$S^* = \delta_d^*/\delta_m^*. \tag{2.5}$$

Here, δ_d^* and δ_m^* represent the displacement and momentum thicknesses of the profiles after being rescaled by the dynamic frame. In figure 3(*c*), the black line denotes the shape factor for the PBP profile, $S \sim 2.47$ in the range $0.026 \leq Pr \leq 0.033$. We observe that S^* is smaller than 2.47 for almost all of our measurements. The difference between the dynamically rescaled temperature profiles and the PBP profile increases with increasing Ra. This is because the BL becomes thinner and more strongly influenced by turbulence, which means that the profile reaches its asymptotic value more slowly (Pandey 2021). Larger deviations are found in the region near the side wall, which is more affected by turbulent fluctuations of the flow. The results in figure 3(*c*) demonstrate that the local thermal BLs are not fully laminar whereby the nature of the BL becomes increasingly transient with growing Ra.

2.3. *Scaling of BL thickness with Ra*

Figure 4 presents the thickness of both the mean thermal and viscous BLs as a function of Ra. The local instantaneous thermal BL $\delta_T(x, t)$ is determined using the slope method, as described in § 2.2. From these data, we then compute the time-averaged value for each Ra, denoted as $\delta_T = \langle \delta_T(x, t) \rangle$. The continuous reduction of the mean thickness of the thermal BL, δ_T, with increasing Ra, is evident for both the shear-dominated region at the plate centre and the position near the side wall. Moreover, the width of the thermal BL is larger near the side wall. The thermal BL thickness is inversely proportional to the vertical diffusive heat flux at the plate, which obviously increases with Ra and is lower near the sidewall than in the shear-dominated region. It has also been reported in previous studies (Wagner *et al.* 2012; Scheel & Schumacher 2014; Pandey 2021) that the variation of the BL width aligns with the direction of the LSC along the plate, in particular, the BL thickness increases in the downstream direction from the plate centre.

We observe different scaling exponents for the two measuring positions under consideration here. While δ_T shows a $Ra^{-0.20}$ scaling at the centre region (in accordance

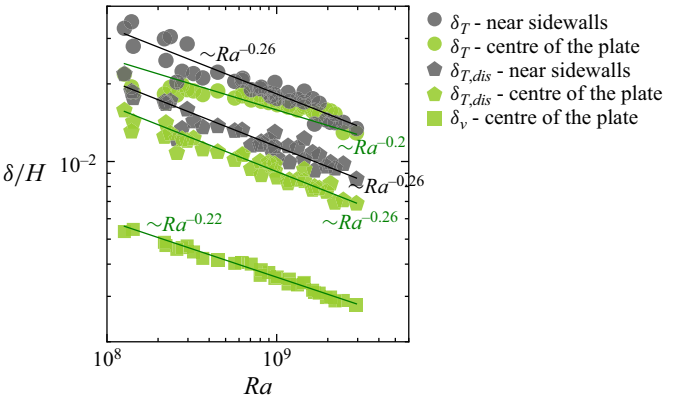

Figure 4. Time-averaged thermal and viscous BL thicknesses as a function of Ra.

with Naert *et al.* 1997), it scales like $Ra^{-0.26}$ near the side wall. The same value of -0.26 has been reported by Scheel & Schumacher (2016) for δ_T averaged over the plate area. Pandey (2021) obtained an exponent of -0.25, also for a horizontally averaged value of δ_T. In view of the aspect that the shear-dominated zone probably only occupies a small part of the total area of the plate, this result is understandable. In our case, the different exponents also mean that the difference in BL thickness between the centre and the side wall region is greatest at low Ra, whereas the thicknesses are similar at high Ra. This observation is consistent with the findings of Pandey (2021), who observed a much steeper decline of δ_T in the ejection region as compared with the shear-domination zone.

Another parameter for characterising BL behaviour is the displacement thickness (Schlichting & Gersten 2016). It provides a measure of the effective thickness of the thermal BL and is defined in a fixed frame as Scheel & Schumacher (2017)

$$\delta_{T,dis} = \int_0^\infty \left(1 - \frac{\bar{T}}{\bar{T}_{bulk}}\right) \mathrm{d}z. \tag{2.6}$$

Scheel & Schumacher (2017) suggest that the displacement thickness scales with $Ra^{-0.25}$ for a laminar BL, whereas it decreases with an exponent of -0.1 for a turbulent BL. It is shown in figure 4 that $\delta_{T,dis}$ decreases with an exponent of -0.26 for both measuring positions. This analysis indicates that our thermal BLs are still in a transitional state and therefore exhibit laminar-like scaling rather than turbulence-like scaling.

Figure 4 also contains the viscous BL thickness, δ_v, for comparison. However, this variable is not directly accessible for direct measurements in our current experimental set-up. Instead, we employ the equation for the Blasius BL thickness (Schlichting & Gersten 2016), defined as $\delta_v = aH/\sqrt{Re_H}$, under the assumption that the viscous BL remains in the laminar regime. Here, the height H is used as the characteristic length for Reynolds number, $Re_H = u_{LSC}H/\nu$. The characteristic LSC velocity, u_{LSC}, is measured as the time-averaged horizontal velocity beneath the top plate by means of the UDV sensors shown in figure 1(*a*) (see also Zürner *et al.* 2019). To determine δ_v and the appropriate coefficient a, we adopt the assumption that the ratio of the thermal BL to the viscous BL remains constant for a given Ra. Shishkina *et al.* (2010) derived the following relationship between the thermal BL and the viscous BL for $3 \times 10^{-4} \leq Pr \leq 3$:

$$\delta_T/\delta_v \sim Pr^{-0.357+0.022\log Pr}. \tag{2.7}$$

Since u_{LSC} is measured at the intersection of the two UDV measuring lines at the centre of the top plate (see figure 1*a*), we input the δ_T data from the centre position into (2.7). The resulting coefficient was found to be $a \sim 0.53$, which is similar to values reported in previous studies: $a = 0.482$ by Grossmann & Lohse (2002) and $a = 0.6$ by Zhou & Xia (2010). The δ_ν data presented in figure 4 decrease with a scaling of $Ra^{-0.22}$. This scaling is consistent with $Re \sim Ra^{0.45}$, which has been identified in many previous studies (Qiu & Tong 2001; Grossmann & Lohse 2002; Ahlers *et al.* 2009; Scheel & Schumacher 2017; Schindler *et al.* 2022; Xu, Zhang & Xia 2022). Consequently, this leads to a Ra dependence of $\delta_\nu \sim Re^{-0.5} \sim Ra^{-0.225}$ in the laminar regime (Shi *et al.* 2012), a value similar to our observed scaling of -0.22. Thus, the authors suggest that, given the limitations of the velocity measurements in the current set-up, the observed scaling of $\delta_\nu \sim Ra^{-0.22}$ is consistent with a laminar BL.

3. Summary and conclusions

The present experimental study is dedicated to the investigation of the thermal BL in turbulent liquid metal RBC, within the Pr range of 0.026 to 0.033 and Ra up to 2.9×10^9. For this purpose, we measure vertical temperature profiles at two positions directly below the top plate. One of the measuring positions is in the centre area of the plate, over which the LSC constantly flows so that a shear-dominated zone can be certainly assumed here. The second thermocouple is installed at a radial distance of $0.33D$ from the centre of the plate. It is well known that the horizontal velocity component of the LSC weakens with increasing distance from the plate centre. In the lateral areas, thermal plumes either form and detach (plume ejection) or impinge (plume impact) when they come from the opposite plate.

Our analysis reveals significant differences in temperature profiles, fluctuation statistics, and BL thickness scaling between the two considered measuring positions. In the shear-dominated region, temperature profiles resemble laminar BL profiles (the PBP profile), whereas in the region near the side wall, stronger fluctuations lead to deviations from the laminar behaviour. These discrepancies become more pronounced at higher Ra indicating an increasing influence of turbulent fluctuations with increasing Ra. In the present study, the viscous BL δ_ν, which, in low-Pr fluids, is significantly smaller than the thermal BL δ_T, could not be measured directly. However, a rough estimate confirms that the viscous BL can be regarded as laminar under the conditions considered here. The much thicker thermal BL, therefore, extends into the zone of turbulent flow and could therefore be directly affected by it. Our results also show this but do not provide evidence for a transition to a fully turbulent thermal BL.

The thermal BL width, δ_T, shows distinct scalings for the centre and side wall regions, $Ra^{-0.20}$ and $Ra^{-0.26}$, respectively. The difference in the BL thickness is most pronounced for small Ra, but the different scaling exponents result in almost the same BL thickness for $Ra \approx 10^9$. The thermal displacement thickness $\delta_{T,dis}$ declines with an exponent of -0.26 in both regions which indicates a behaviour akin to a laminar BL. This appears to be contrasted by the deviations of our data from the characteristic value of the shape factor S^* for a PBP profile even after the application of dynamic rescaling. However, only minor deviations occur in the shear-dominated zone, whereas significantly lower values were determined for the side wall region at high Ra. The thermal BL profiles deviate from the PBP profile in both regions, with larger discrepancies found in the side wall region where stronger turbulent fluctuations occur frequently. This suggests that a possible departure from the laminar state to a transitional or even turbulent BL is most likely to

occur first in the side wall region. Growing turbulent fluctuations with increasing *Ra* affect the laminar character of the thermal BL. However, according to the findings in this study, the BL does not yet become fully turbulent but shows a transitional behaviour in the area near the side wall at high *Ra*. The larger local BL width in the side-wall region corresponds to the formation and detachment of coarser plumes resulting in a less steep vertical temperature gradient in the side-wall region compared with the centre region (Pandey 2021) (see figure 3). It is interesting to note that our experimental findings agree very well with the numerical results of Pandey (2021), although due to the volatile nature of the LSC, our measurements at the sidewall represent a time average over the BL behaviour in different areas (ejection, impact, laterally with respect to the LSC plane), whereas the analysis by Pandey (2021) fits exactly in the LSC direction. We assume that measurements focusing explicitly on the ejection zone could reveal even more pronounced deviations from a laminar BL. Therefore, in further experiments, we plan to increase the number of temperature measurement points in the near-wall region and combine this with simultaneous velocity measurements to determine the instantaneous LSC direction and localise the ejection zone. The continuation of these experiments will provide valuable insights into the thermal BL dynamics in turbulent liquid metal convection, contributing to a better understanding of the heat transfer mechanism.

Acknowledgements. We thank the anonymous reviewers for their valuable comments and suggestions.

Funding. The authors acknowledge financial support from the Deutsche Forschungsgemeinschaft (DFG) with grants no. EC 217/5-1 and no. VO 2331/1-1.

Declaration of interests. The authors report no conflict of interest.

Author ORCIDs.
Nayoung Kim https://orcid.org/0000-0003-4928-8730;
Felix Schindler https://orcid.org/0000-0003-2123-0430;
Tobias Vogt https://orcid.org/0000-0002-0022-5758;
Sven Eckert https://orcid.org/0000-0003-1639-5417.

References

Ahlers, G., Grossmann, S. & Lohse, D. 2009 Heat transfer and large scale dynamics in turbulent Rayleigh–Bénard convection. *Rev. Mod. Phys.* **81** (2), 503.

Bodenschatz, E., Pesch, W. & Ahlers, G. 2000 Recent developments in Rayleigh–Bénard convection. *Annu. Rev. Fluid Mech.* **32** (1), 709–778.

Castaing, B., Gunaratne, G., Heslot, F., Kadanoff, L., Libchaber, A., Thomae, S., Wu, X.-Z., Zaleski, S. & Zanetti, G. 1989 Scaling of hard thermal turbulence in Rayleigh–Bénard convection. *J. Fluid Mech.* **204**, 1–30.

Chillà, F. & Schumacher, J. 2012 New perspectives in turbulent Rayleigh–Bénard convection. *Eur. Phys. J.* E **35**, 1–25.

Ching, E.S.C., Leung, H.S., Zwirner, L. & Shishkina, O. 2019 Velocity and thermal boundary layer equations for turbulent Rayleigh–Bénard convection. *Phys. Rev. Res.* **1** (3), 033037.

Grossmann, S. & Lohse, D. 2000 Scaling in thermal convection: a unifying theory. *J. Fluid Mech.* **407**, 27–56.

Grossmann, S. & Lohse, D. 2002 Prandtl and Rayleigh number dependence of the Reynolds number in turbulent thermal convection. *Phys. Rev.* E **66** (1), 016305.

Horanyi, S., Krebs, L. & Müller, U. 1999 Turbulent Rayleigh–Bénard convection in low Prandtl–number fluids. *Intl J. Heat Mass Transfer* **42** (21), 3983–4003.

Naert, A., Segawa, T. & Sano, M. 1997 High-Reynolds-number thermal turbulence in mercury. *Phys. Rev.* E **56** (2), R1302–R1305.

Niemela, J.J., Skrbek, L., Sreenivasan, K.R. & Donnelly, R.J. 2000 Turbulent convection at very high Rayleigh numbers. *Nature* **404** (6780), 837–840.

PANDEY, A. 2021 Thermal boundary layer structure in low-Prandtl-number turbulent convection. *J. Fluid Mech.* **910**, A13.

VAN DER POEL, E.P., OSTILLA-MÓNICO, R., VERZICCO, R., GROSSMANN, S. & LOHSE, D. 2015 Logarithmic mean temperature profiles and their connection to plume emissions in turbulent Rayleigh–Bénard convection. *Phys. Rev. Lett.* **115** (15), 154501.

QIU, X.-L. & TONG, P. 2001 Onset of coherent oscillations in turbulent Rayleigh–Bénard convection. *Phys. Rev. Lett.* **87** (9), 094501.

RAYLEIGH, LORD 1916 LIX. On convection currents in a horizontal layer of fluid, when the higher temperature is on the under side. *Lond. Edinb. Dublin Phil. Mag. J. Sci.* **32** (192), 529–546.

VAN REEUWIJK, M., JONKER, H.J.J. & HANJALIĆ, K. 2008 Wind and boundary layers in Rayleigh–Bénard convection. I. Analysis and modeling. *Phys. Rev.* E **77** (3), 036311.

SAMUEL, R.J., BODE, M., SCHEEL, J.D., SREENIVASAN, K.R. & SCHUMACHER, J. 2024 Boundary layers in thermal convection are fluctuation-dominated. Preprint, arXiv:2403.12877.

SCHEEL, J.D., KIM, E. & WHITE, K.R. 2012 Thermal and viscous boundary layers in turbulent Rayleigh–Bénard convection. *J. Fluid Mech.* **711**, 281–305.

SCHEEL, J.D. & SCHUMACHER, J. 2014 Local boundary layer scales in turbulent Rayleigh–Bénard convection. *J. Fluid Mech.* **758**, 344–373.

SCHEEL, J.D. & SCHUMACHER, J. 2016 Global and local statistics in turbulent convection at low Prandtl numbers. *J. Fluid Mech.* **802**, 147–173.

SCHEEL, J.D. & SCHUMACHER, J. 2017 Predicting transition ranges to fully turbulent viscous boundary layers in low Prandtl number convection flows. *Phys. Rev. Fluids* **2** (12), 123501.

SCHINDLER, F., ECKERT, S., ZÜRNER, T., SCHUMACHER, J. & VOGT, T. 2022 Collapse of coherent large scale flow in strongly turbulent liquid metal convection. *Phys. Rev. Lett.* **128** (16), 164501.

SCHLICHTING, H. & GERSTEN, K. 2016 *Boundary-Layer Theory*. Springer.

SCHUMACHER, J., BANDARU, V., PANDEY, A. & SCHEEL, J.D. 2016 Transitional boundary layers in low-Prandtl-number convection. *Phys. Rev. Fluids* **1** (8), 084402.

SHI, N., EMRAN, M.S. & SCHUMACHER, J. 2012 Boundary layer structure in turbulent Rayleigh–Bénard convection. *J. Fluid Mech.* **706**, 5–33.

SHISHKINA, O., HORN, S., WAGNER, S. & CHING, E.S.C. 2015 Thermal boundary layer equation for turbulent Rayleigh–Bénard convection. *Phys. Rev. Lett.* **114** (11), 114302.

SHISHKINA, O., STEVENS, R.J.A.M., GROSSMANN, S. & LOHSE, D. 2010 Boundary layer structure in turbulent thermal convection and its consequences for the required numerical resolution. *New J. Phys.* **12** (7), 075022.

SHISHKINA, O. & THESS, A. 2009 Mean temperature profiles in turbulent Rayleigh–Bénard convection of water. *J. Fluid Mech.* **633**, 449–460.

SHRAIMAN, B.I. & SIGGIA, E.D. 1990 Heat transport in high-Rayleigh-number convection. *Phys. Rev.* A **42** (6), 3650.

SIGGIA, E.D. 1994 High Rayleigh number convection. *Annu. Rev. Fluid Mech.* **26** (1), 137–168.

STEVENS, R.J.A.M., ZHOU, Q., GROSSMANN, S., VERZICCO, R., XIA, K.-Q. & LOHSE, D. 2012 Thermal boundary layer profiles in turbulent Rayleigh–Bénard convection in a cylindrical sample. *Phys. Rev.* E **85** (2), 027301.

SUN, C., CHEUNG, Y.-H. & XIA, K.-Q. 2008 Experimental studies of the viscous boundary layer properties in turbulent Rayleigh–Bénard convection. *J. Fluid Mech.* **605**, 79–113.

TAI, N.C., CHING, E.S.C., ZWIRNER, L. & SHISHKINA, O. 2021 Heat flux in turbulent Rayleigh–Bénard convection: predictions derived from a boundary layer theory. *Phys. Rev. Fluids* **6** (3), 033501.

WAGNER, S., SHISHKINA, O. & WAGNER, C. 2012 Boundary layers and wind in cylindrical Rayleigh–Bénard cells. *J. Fluid Mech.* **697**, 336–366.

WANG, Y., HE, X. & TONG, P. 2016 Boundary layer fluctuations and their effects on mean and variance temperature profiles in turbulent Rayleigh–Bénard convection. *Phys. Rev. Fluids* **1** (8), 082301.

WANG, Y., XU, W., HE, X., YIK, H., WANG, X., SCHUMACHER, J. & TONG, P. 2018 Boundary layer fluctuations in turbulent Rayleigh–Bénard convection. *J. Fluid Mech.* **840**, 408–431.

WONDRAK, T., SIEGER, M., MITRA, R., SCHINDLER, F., STEFANI, F., VOGT, T. & ECKERT, S. 2023 Three-dimensional flow structures in turbulent Rayleigh–Bénard convection at low Prandtl number $Pr = 0.03$. *J. Fluid Mech.* **974**, A48.

WU, X.-Z. & LIBCHABER, A. 1992 Scaling relations in thermal turbulence: the aspect-ratio dependence. *Phys. Rev.* A **45** (2), 842.

XU, F., ZHANG, L. & XIA, K.-Q. 2022 Three-dimensional properties of the viscous boundary layer in turbulent Rayleigh–Bénard convection. *J. Fluid Mech.* **947**, A15.

ZHOU, Q., STEVENS, R.J.A.M., SUGIYAMA, K., GROSSMANN, S., LOHSE, D. & XIA, K.-Q. 2010 Prandtl–Blasius temperature and velocity boundary-layer profiles in turbulent Rayleigh–Bénard convection. *J. Fluid Mech.* **664**, 297–312.

ZHOU, Q., SUGIYAMA, K., STEVENS, R.J.A.M., GROSSMANN, S., LOHSE, D. & XIA, K.-Q. 2011 Horizontal structures of velocity and temperature boundary layers in two-dimensional numerical turbulent Rayleigh–Bénard convection. *Phys. Fluids* **23** (12), 125104.

ZHOU, Q. & XIA, K.-Q. 2010 Measured instantaneous viscous boundary layer in turbulent Rayleigh–Bénard convection. *Phys. Rev. Lett.* **104** (10), 104301.

ZHOU, Q. & XIA, K.-Q. 2013 Thermal boundary layer structure in turbulent Rayleigh–Bénard convection in a rectangular cell. *J. Fluid Mech.* **721**, 199–224.

ZÜRNER, T., SCHINDLER, F., VOGT, T., ECKERT, S. & SCHUMACHER, J. 2019 Combined measurement of velocity and temperature in liquid metal convection. *J. Fluid Mech.* **876**, 1108–1128.